LIGO-T960212-A-D

HYTEC-TN-LIGO-04a
07/10/96
revision *a*, 10/31/96

Design of Vacuum Compatible Damped Metal Springs for Passive Vibration Isolation of the LIGO detectors

Eric Ponslet
July 10, 1996
Revision *a*, October 31st, 1996

Abstract

This note describes the design of damped metal springs for vibration isolation of the LIGO detectors. Previous studies have shown that metal springs have the potential of increasing the static load capacity to dynamic stiffness ratio by large factors compared to the VITON springs used in the 40 meter prototype, leading to very substantial improvements in isolation performance. The main design challenge is related to the requirement that any damping treatments used (viscoelastic materials for example) be completely isolated from the high vacuum environment inside the detector chambers. Various damping concepts have been considered and have led to two promising spring designs: a multi-layer tubular coil spring and a semi-circular leaf spring, both using viscoelastic constrained layer damping. Both designs completely enclose the viscoelastic material inside the metal spring. This note describes the design, analysis, and optimization of those two springs. As this note is being written, prototypes are not yet available and experimental results are therefore not included.

HYTEC Inc.
110 Eastgate Dr.
Los Alamos, NM 87544
(505) 662-0080

LIGO PROJECT

1. Motivation

The first generation of LIGO detectors will be isolated from seismic vibrations by a passive, multi-stage isolation stack consisting of successive layers of compliant elements (springs) with damping and rigid masses. Neglecting damping, the vertical isolation performance of a symmetric stack can be evaluated using a one-dimensinal approximation as shown in Fig. 1 (in a fashion similar to a multi-stage LC electronic filter).

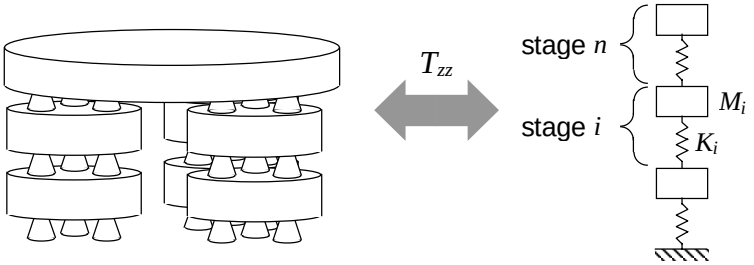

Figure 1: Approximation for vertical-vertical isolation performance of an *n*-stage stack.

We have previously shown[1] that the vertical-vertical transmissibility $T_{zz}(f)$ at frequency f of a stack with n stages is assymptotically equal to

$$T_{zz}(f) \approx \left(\frac{f_1 \cdots f_i \cdots f_n}{f^n} \right)^2 \geq \left(\frac{g}{4\pi^2 f^2 \delta_{\max}} \right)^n, \qquad (1)$$

where

$$f_i = \frac{1}{2\pi} \sqrt{\frac{K_i}{M_i}} \qquad (2)$$

is the uncoupled natural frequency of stage i, g is the acceleration of gravity, and

$$\delta_{\max}(f) = \frac{P_{\max}}{|k_{ax}(f)|} \qquad (3)$$

is a ***frequency dependent quantity*** defined as the ratio of the static load capacity $P_{\max}$ of the springs used in the stack to the norm of their axial (vertical) dynamic stiffness $k_{ax}(f)$ at frequency f. We will refer to this parameter $\delta_{\max}$ as the ***characteristic deflection*** of the spring at a frequency f. Equation (1) shows that the ultimate vertical isolation performance $T_{zz}^{\min}(f)$ that can be achieved with a stack of a given number of stages is only a function of the characteristic deflection of the springs. This is also illustrated in Fig. 2 where the best achievable vertical isolation performance at 35 Hz of a 4 stage symmetric stack is plotted as a function of the characteristic deflection of its springs.

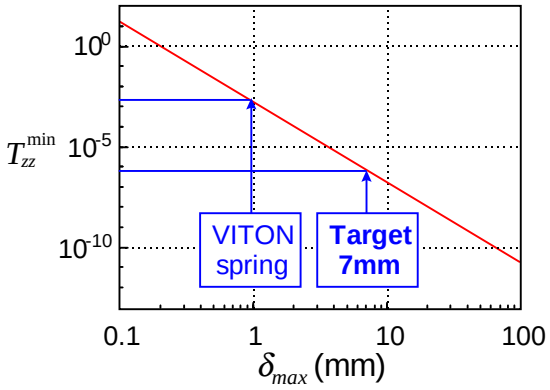

Figure 2: Best achievable vertical isolation at 35 Hz with a 4 stage symmetric stack as a function of δ_{max}.

The current fall-back design solution for the LIGO seismic isolation stacks uses VITON rubber springs identical to those used in the 40 meter prototype at CalTech. Unfortunately, because of their static deflection mechanism (direct axial compression) and the limited stress capacity of VITON, the characteristic deflection δ_{max} of those springs is very small (about 0.96 mm or 0.038 in. at 35 Hz), leading to insufficient isolation of the test masses. Figure 3 compares the predicted vertical-vertical transmissibility of an optimized VITON-based BSC isolation system with the corresponding design requirement[2].

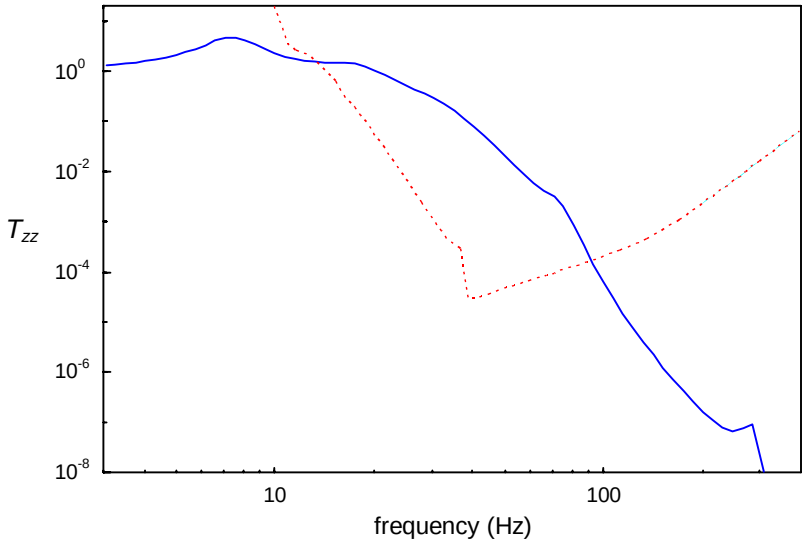

Figure 3: Vertical transmissibility of a 4-stage VITON-based BSC isolation stack (—) compared to design requirement (---).

We can see that the requirement on T_{zz} is violated by up to 3.5 orders of magnitude at 35 Hz. References [1] and [3] have shown that varying the number of stages or the stack design (distribution of stage masses) cannot improve on this situation. However, Fig. 2 and reference [3] indicate that very large improvements in isolation performance can be achieved with even moderate increases in spring characteristic deflection. Looking at Fig. 2 or Eq. 1, we see that a factor 10 increase in δ_{max} leads to 4 orders of magnitude

improvement in the vertical transmissibility of a 4 stage stack. Since the required improvement is about 3.5 orders of magnitude, we conclude that **a spring with a δ_{max} at 30 to 40 Hz of roughly $\sqrt[4]{10^{3.5}} \times 0.96 \approx 7$ mm could lead to stacks that satisfy the isolation requirements**. This is all very approximate since it is based on axial stiffness of the springs and vertical transmissibility only. In the actual stack, shear stiffness, horizontal transmissibility, and coupling terms also contribute to final performance.

In addition, uncertainties on the long term mechanical behavior of baked VITON springs under large static loads, as well as the large creep of those springs over time (20% contraction in a year) and thermal sensitivity makes them somewhat undesirable for use in the LIGO isolation stacks.

We also note that commercially available coil springs roughly the size of the VITON springs easily give characteristic deflections in excess of 30 mm[4], leading to stacks with isolation performance largely in excess of requirements[3]. These springs however are undamped which leads to unacceptable responses to transients and low frequency excitations.

These observations lead one to expect that metal springs might be designed with embedded damping treatments for transient and low frequency response, and still have characteristic deflections large enough to satisfy isolation requirements.

2. Design Requirements

2.1 Vacuum Compatibility

The springs must be compatible with the high vacuum environment of the detector chambers. This implies low outgassing rates but more importantly the absence of any vaporizable contaminants that might condense on the mirrors of the interferometer and get baked on their surface by the laser beams. These requirements[5] limit the choice of materials that can be used for the springs and force complete enclosure of any viscoelastic materials within the metal structure. This is a very important restriction that has wide implications on spring design and complexity.

2.2 Specific Deflection (Static Load Capacity and Dynamic Axial Stiffness)

The specific deflection of the springs (δ_{max}, ratio of static load capacity to dynamic axial stiffness, frequency dependent quantity) should be maximized. This directly leads to maximum vertical isolation performance of any stack built with those springs. As shown in Section 1 of this document, a rough lower limit on δ_{max} is about 7 mm around 30 to 40 Hz: any spring design that satisfies this limit can be expected to lead to stacks that satisfy vertical isolation requirements.

2.3 Shear stiffness

The requirement on specific deflection only guarantees good isolation performance in the vertical direction. Horizontal isolation is much more difficult to predict (full 3D modeling is required because of complex coupling between modes) and is controlled by exact stack geometry and both axial and shear stiffnesses of the springs. Although the effect of shear stiffness on horizontal performance is neither easily predictable or even

monotonic, there is a general tendency for performance to improve when shear stiffness is reduced[3]. For this reason, it is reasonable to impose as a weak objective to minimize the ratio of shear to axial stiffness k_{sh}/k_{ax} (the ratio k_{sh}/k_{ax} is about 0.17 for the VITON springs and 0.4 for typical heavy duty steel compression springs). We must also keep in mind that, as k_{sh}/k_{ax} is reduced, lateral buckling of the springs under the static load becomes an issue.

2.4 Damping

For isolation performance, damping should be kept to a minimum since it typically leads to stiffening of the springs with increasing frequency (viscoelastic damping). On the other hand, limiting response amplitudes around the stack resonant frequencies (frequency range 1 to 20 Hz) and response to transients require some amount of damping in the springs. Based on previous experience with the 40 meter prototype and interpretation of low frequency response requirements[2], a conservative lower limit on the spring loss factor (both in the axial and shear directions) of about 3% at room temperature and in a frequency range from 1 to 20 Hz is adopted. For simplification, a single "target" frequency of 10 Hz will be used in this study. The damping requirement can then be written

$$\eta\ (25°\text{C},\ 10\ \text{Hz}) > 3\% \qquad (4)$$

2.5 Size

Larger springs lead to taller isolation stacks. In the BSC, this leads to a longer and heavier downtube structure, leading to heavier stack elements and an even taller stack, and so on… In the HAM, the total vertical space available for the support structure, stack, and optical table is very limited so that stack height should be kept to a minimum. Horizontal space available on the leg elements is also limited. An arbitrary limit on the spring size, corresponding to about twice that of the VITON springs will be imposed: the springs should fit within a cylinder 8 cm in diameter by 8 cm high when statically loaded at full capacity.

2.6 Static Load Capacity

We have shown in [3] that the springs should have a load capacity small enough to minimize the effects of discreteness (i.e. since the number of springs at each stage is discrete, they can be used close to 100% of their capacity only if each stage uses at least a few of them). A reasonable range is 100 lbs (445 N) < P_{max} < 300 lbs (1334 N), with an ideal value of 125 lb (556 N) that makes the metal springs direct 1 to 1 replacements for the VITON springs (because of tight schedules, preliminary stack design will take place before completion of the metal spring development efforts and will therefore be based on VITON springs).

2.7 First Resonant Frequency

Internal resonances in the spring can be excited by residual seismic perturbations. These resonances would create peaks in the transmissibility curves above the "ideal" stack response. The lowest resonant frequency of a spring "clamped" between two fixed leg elements should then be kept high enough that the corresponding response peaks do not significantly affect performance. Considering the steep response roll-off of a four-stage stack (about 160 dB/decade, see [1] and Fig. 3), resonant frequencies above say 250 Hz are

not likely to deteriorate performance enough to violate requirements: the margin at 250 Hz would be about 8 orders of magnitude for a stack that satisfies isolation requirements. Note also that, since the springs will be designed with embedded damping, internal resonances are likely to have loss factors of the order of a few percent, limiting the amplification ratio (or quality factor, *Q*) to less than 100.

2.8 Acoustic Transmission

Acoustic transmission is not an issue with VITON springs because the material itself is lossy enough to provide sufficient attenuation. This is not necessarily the case with a metal spring, even when damping treatments are used: the damping treatments are designed to dissipate energy for macroscopic (global) spring deflections but direct acoustic transmission along the metal enclosure is not excluded. However, acoustic transmission is difficult to predict for complex multi-phase structures like the designs presented in this document. Acoustic qualification of the metal springs is therefore likely to rely mostly on testing. Short of other solutions, small acoustic pads made of VITON may have to be inserted between the springs and leg masses, as shown in Sections 5.6 and 6.4.

3. Damping Mechanisms

A number of damping mechanisms are listed below. Some of those have been considered but only viscoelastic damping was judged acceptable.

3.1 Laminar Air Flow Damping

Double chamber air springs are commonly used for high performance vibration isolation. Air circulation from one chamber to the other is restricted by a porous medium. The energy loss through the porous medium provide damping to the air spring. Although very appealing isolation performance can be achieved with this type of springs (natural frequencies down to about 1 Hz), the large volume of air they contain makes their height very sensitive to small temperature variations[6]. Without the use of complex compensation techniques, this is incompatible with the extreme positional stability required for the LIGO detectors.

3.2 Viscous Fluid Damping

Use of a fluid to provide damping is excluded because of the high risk of catastrophic leaks into the vacuum chambers. Also, being proportional to frequency, viscous damping is detrimental to the rolloff rate of transmissibility (20 dB/decade/stage with viscous damping instead of 40 dB/decade/stage with structural damping).

3.3 Shape Memory Alloys, Magneto-Elastic Alloys, …

These classes of metallic alloys have particularly high structural damping compared to other metals. Loss factors up to a few percent can be achieved. However, for both classes of materials, the loss factor is very dependent on alternating stress amplitude and tends to very small values at vanishingly small alternating stresses[7,8,9]. In addition, static stresses superposed on alternating stresses reduce damping even further. Springs designed for the LIGO isolation would clearly be in the worst possible operating conditions: they

must support large static loads and see only extremely small oscillations due to seismic excitation.

3.4 Viscoelastic Materials

A wide selection of rubbers, plastic, and plastic alloys exhibit this type of damping. Damping forces are neither proportional to deformation (ideal structural damping) nor to deformation rate (ideal viscous damping). Rather, there is a complex, frequency and temperature dependent relation between damping forces and deformations. This behavior is usually modeled using a *complex stiffness* approach where the shear modulus G of a material is a complex quantity

$$G = G' + iG'' = G'(1 + i\eta), \qquad (4)$$

where $i = \sqrt{-1}$, the *loss factor* η is the ratio of the real to the imaginary part of the modulus, and all other quantities vary rapidly with temperature and frequency. *G'* and *G"* are called storage and loss moduli, respectively. Using temperature-frequency equivalence principle, these material properties are typically reduced to a nomograph that gives the storage modulus *G'* and the loss factor η as functions of both temperature and frequency. An typical nomograph is shown in Fig. 4.

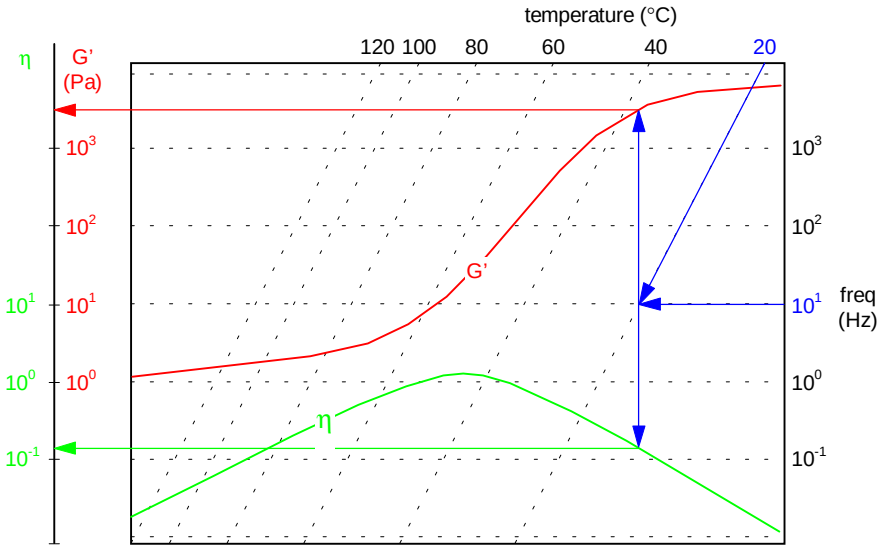

Figure 4: Typical nomograph for temperature and frequency dependent properties of viscoelastic materials.

Most viscoelastic materials have outgassing rates and products that are incompatible with the vacuum environment of the LIGO detectors and must be completely enclosed in a vacuum compatible material (like an all-metal shell for example).

4. Viscoelastic-Filled Tubular Coil Spring

This section presents the simplest conceptual design of a damped coil spring: a coiled compression spring with a metallic tubular cross section, filled with a high damping

viscoelastic material. It will be shown that this concept is incapable of providing loss factors even approaching the required 3%.

4.1 Concept

Helical coil springs offer very large static deflection capacity relative to their size. This is due to the uniform torsional loading of the spring wire along its length and the lever arm effect from the coil radius. One of the simplest ways to introduce viscoelastic damping in a coil spring in a way that the viscoelastic material is completely shielded from the vacuum consists of coiling a length of metal tube into a compression spring and - after any required heat-treatment, fill the tube with a thermoset or thermoplastic viscoelastic material. The ends of the tube could then be closed with welded metal caps.

4.2 Analysis

4.2.1 General coil spring relations

A coiled compression spring (Fig. 5) is defined by the cross-sectional geometry and material properties of its "wire", its mean coil diameter *D*, pitch *p*, and number of turns *n* in the coil (neglecting end-turns so *n* is also the number of *active* turns).

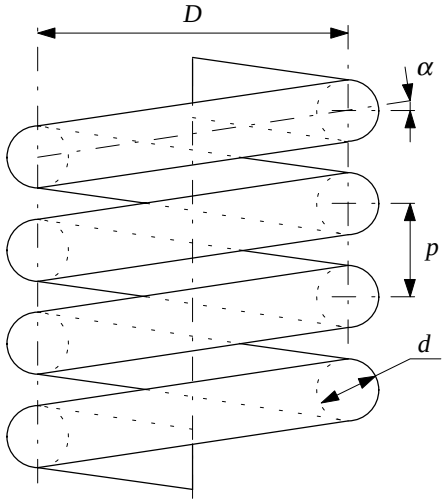

Figure 5: Coil spring dimensions

For springs with circular cross section "wire" the *spring index* $c = D/d$ is defined as the ratio of the mean coil diameter to the cross-section diameter. It is a measure of the tightness of the coil. The *pitch angle* $\alpha = \tan^{-1}\left(p/\pi D\right)$ is the angle made by the "wire" with the longitudinal axis of the coil.

Springs with reasonably large index ($c > 5$) and small pitch angle ($\alpha < 12°$) under axial loading can be analyzed with good accuracy by assuming the "wire" cross section to behave like a straight torsion bar under a twisting moment $T = PD/2$, where P is the compression load on the spring. This leads to the axial stiffness

$$k_{ax} = \frac{4k_t}{n\pi D^3}, \qquad (5)$$

where k_t is the torsional stiffness of the "wire" cross section. Note that for a solid circular cross section of diameter *d*, of a material with shear modulus *G*, the section torsional stiffness $k_t = \pi G d^4 / 32$ leads to the classical relation

$$k_{ax} = \frac{G d^4}{8 n D^3}. \qquad (6)$$

4.2.2 Dynamic behavior

Equation (5) can be used for any cross-sectional geometry. For a thin-wall tubular cross-section of diameter *d*, wall thickness *t*, and shear modulus G_w (and negligible damping), filled with a viscoelastic material with shear storage modulus G_v' and loss factor η_v (Fig. 6) the torsional stiffness can be written as the complex number

$$k_t = k_t'(1 + i\eta_t) = \frac{\pi d^3 t G_w}{4} + \frac{\pi d^4 G_v'(1 + i\eta_v)}{32}. \qquad (7)$$

Note that both G_v' and η_v are - in general - frequency and temperature dependent properties (Section 3.4)

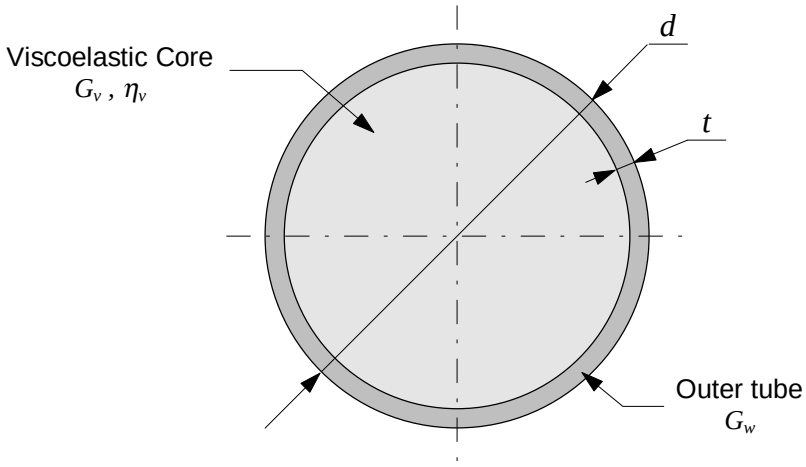

Figure 6: Cross-section of viscoelastic filled coil spring.

From Eq. (7), we can extract the torsional loss factor

$$\eta_t = \Im m(k_t) / \Re e(k_t) = \frac{G_v' d}{G_v' d + 8 G_w t} \eta_v, \qquad (8)$$

and note that by virtue of Eq. (5), it is equal to the net axial loss factor η_{ax} of the coil spring.

This last equation shows that $\eta_{ax} \le \eta_v$ by a factor equal to the ratio of core torsional stiffness to total section torsional stiffness. Because viscoelastic materials are typically soft compared to metals, the core can only participate a relatively small fraction of the cross-section torsional stiffness. This implies that the net spring loss factor η_{ax} will be much smaller than the core loss factor η_v and indicates that the required 3% loss factor is likely to be difficult to achieve with this design concept.

4.2.3 Static load capacity

To evaluate static load capacity, we conservatively assume that creep is unlimited in the viscoelastic core, ultimately forcing the outer tube to carry 100% of the applied load *P*. In these conditions, the shear stress τ_w in the wall of the tube is

$$\tau_w = \frac{2PD}{\pi d^2 t} \qquad (9)$$

This is usually referred to as the *uncorrected* stress because it does not account for the slight non-uniformity of stress distribution due to the curvature of the "wire"; however the error associated with this approximation is small for spring indices $c \geq 5$ after stress redistribution through local yielding has occurred[10,11]. Adopting a conservative design practice for solid wire coiled compression springs under primarily static loads[10,11], we require that τ_w be limited to 35% of the outer tube material tensile strength σ_{tensile}, i.e.

$$\tau_w \leq \tau_w^{\max} = 0.35 \times \sigma_{tensile}\,. \qquad (10)$$

4.3 Tube Material Selection and Sizing

Since filling the tubular cross section may be done after coiling, an age-hardenable alloy was selected for the tube: the coil can be shaped in the pliable annealed condition and then age hardened at high temperature before filling with the viscoelastic core material. Beryllium copper is such a material. It can be age hardened at temperatures between 600 and 700 °F for 1 to 3 hours. The mechanical properties obtained after age hardening are appropriate for spring design: Young's modulus E_w=128 GPa, shear modulus G_w=47.4 GPa and tensile strength in excess of 1.3 GPa. This gives a maximum allowable shear stress $\tau_w^{\max}$ of about 4.6×10^8 Pa.

Maximizing static deflection with limits on shear stresses, natural frequencies, and spring index leads to a rough initial sizing for the coil spring: a 9.0 mm OD beryllium copper tube with 0.5 mm wall, and 50 mm mean coil diameter can take a 556N axial load (125lb) with a maximum shear stress of about 4.4×10^8 Pa, well below our maximum design stress $\tau_w^{\max}$.

Pitch and number of active coils have no effect (within this approximation) on this stress level and can be chosen to provide sufficient static deflection to yield and enough clearance between coils.

4.4 Viscoelastic Material

Looking at Eq. (8) it is clear that achieving substantial amounts of damping with this design would require a very stiff and very heavily damped material for the core. Substituting *d* and *t* for their values from the previous section and requiring that the net spring loss factor be at least 3% at room temperature and 10 Hz (see Section 2.4), we find

$$\frac{G_v' \eta_v}{G_v' + 0.444 G_w} \geq 3\%\,. \qquad (11)$$

Noticing that, for plastics and rubber type materials $G_v' << G_w$ so that the first term in the denominator of (11) can be neglected, we get the following - very approximate - condition on the shear loss modulus of the core

$$G_v''(25°\,\mathrm{C},10\mathrm{Hz}) = G_v'\eta_v(25°\,C,10\,Hz) \geq 630\,\mathrm{MPa}. \qquad (12)$$

This is a ***very*** demanding condition: most commercially available damping materials (with loss factors of the order of 100% at room temperature and 10Hz) have much softer loss moduli (typically 1 to 50 Mpa), while stiffer high damping plastic materials (filled nylons for example) have storage moduli in the GPa range but much lower loss factors (1 to 3% typical). Table 1 lists a number of high damping materials and their ***approximate*** properties at room temperature and 10 Hz. Note that not all of these materials can even be molded or injected into the coiled tube (because they are only available in sheet form for example).

material	G_v' (MPa)	η_v %	G_v'' (MPa)	remarks
Soundcoat® DYAD 606[12]	22	105	23	sheet form only, resin
Soundcoat® DYAD 609[12]	320	23	74	sheet form only, resin
Sorbothane®, 70 durometer[13]	1	50	0.5	high damping rubber, can be molded
EAR Isodamp® C2003[14]	133	80	106	fused thermoplastic alloy
EAR Isodamp® C1100[14]	17	100	17	thermoplastic alloy, can be molded
EAR Isodamp® SD[14]	400	70	280	sheet form only
EAR Isodamp® CN[14]	233	80	186	extruded thermoplastic, sheet form only
GE-SMRD 100F90[15]	69	90	62	not produced anymore
Viton, 70 durometer[16]	17	37	6	can be molded
LNP Stat-Loy® M[17]	600	5	30	polypropylene
LNP Lubriloy™ R[17]	810	3	24	lubricated nylon 6/6 alloy
LNP Lubriloy™ RA[17]	980	3	29	aramid fiber reinforced nylon
LNP Thermocomp® KFX 1005[17]	2700	0.8	22	short glass fiber reinf. acetal
LNP Verton® MFX-7008[17]	2000	2.5	50	long glass fiber reinf. polypropylene

Table 1: Approximate (some estimated) properties of various viscoelastic materials at 10Hz and room temperature.

To get a better idea of the amounts of damping that can be achieved with this filled tubular coil spring concept, we evaluate Eq. (8) as a function of G_v' and η_v for a beryllium copper tube with d = 9 mm and t = 0.5 mm. The results are shown in the form of iso-damping curves in a (η_v, G_v') chart in Fig. 7. The materials of Table 1 are also marked in the Figure. The loss factors are clearly insufficient: the largest loss achieved is just below 1% using the properties of EAR Isodamp SD, which is not available is a moldable form. Of the moldable compounds, the best performance is achieved with LNP Verton MFX-7008, a glass fiber reinforced polypropylene, which gives only about 0.2% loss factor. We can only conclude that a filled coil spring cannot provide the required damping because existing materials are either stiff with very low damping (plastics) of have high loss factor but insufficient stiffness.

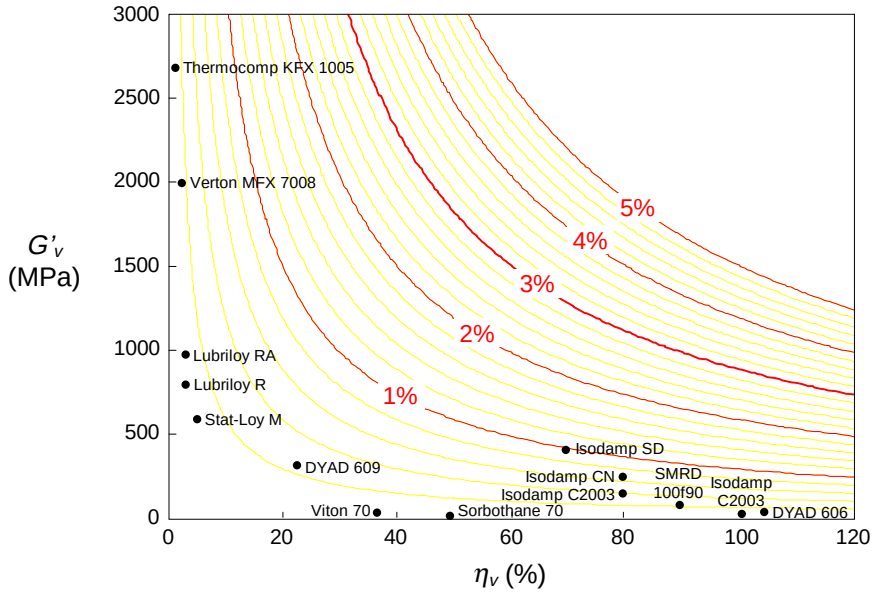

Figure 7: Iso-damping curves for the net loss factor at room temperature and 10 Hz in a beryllium copper tube (9mm OD by 0.5mm wall) filled with a viscoelastic material with shear storage modulus G_v' and loss factor η_v. Damping materials from Table 1 are marked.

5. Multi-Layer Tubular Coil Spring with Constrained Layer Damping

5.1 Concept

Section 4 has shown that a simple filled tubular coil spring is unable to produce the required amount of damping. To achieve larger loss factors using existing viscoelastic materials, we have to amplify the mechanical coupling between the load bearing structure (the outer tube) and the viscoelastic material. In other words, the viscoelastic material must be designed into the spring in a way that it sees large shear strains in response to very small deformations of the spring. Constrained Layer Damping (CLD) can achieve this. It consists of inserting a very thin layer of viscoelastic material between the load bearing structure and a stiff constraining layer. Small relative motion between the load bearing and constraining surfaces induce large shear strain through the thickness of the thin viscoelastic layer.

CLD is traditionally used to damp plate and shell type structures: a thin viscoelastic sheet with a thin metal backing sheet is glued directly on the structure. This concept must be adapted for use in the proposed tubular coil spring, in particular to avoid any exposure of the viscoelastic layer to the vacuum environment. A natural (if complicated) solution is to apply the damping treatment and constraining layer on the *inside* of the load carrying tube. The ends of the tube can be capped to completely enclose the damping material. The most natural configuration then consists of a continuous inner tube (the constraining layer) wrapped in a thin layer of viscoelastic material and trapped inside the outer load bearing tube (manufacturing issues will be addressed further, let us just say for now that the outside tube could be swaged around the inside tube and visco

layer, before coiling). Since a coil spring is essentially a torsion bar, a twisting moment applied to the ***outer*** tube induces a twist angle differential between the inside and outside tube, shearing the viscoelastic layer. If the viscoelastic layer is thin, the shear strains are large and significant amounts of mechanical energy are dissipated into heat.

Although this concept is adequate for a ***straight*** torsion bar, it cannot provide damping in a coil spring because of geometric coupling between the outside and inside tubes. When a coil spring is compressed, the pitch of the helix is reduced. This reduction in pitch geometrically dictates the twist angles of every section along the spring "wire". In a 3 layer CLD spring, since the inner tube is captive inside the outer tube, the twist angles are the same in both, and shear through the thickness of the viscoelastic layer does not appear. We could also say that in a ***coiled*** 3 layer CLD torsion bar the twisting moment is transferred from the outside to the inside tube through compression/traction stresses in the viscoelastic layer instead of shear.

Shear stresses in the viscoelastic layer can be recovered if we eliminate (or largely reduce) geometric coupling by using a series of "short" (much shorter than a full turn of the coil) sections of constraining tube instead of a continuous one, as shown in Fig. 8. The rubber core shown in the figure is only intended to provide internal support to the cross section during coiling. Its effect on mechanical behavior will be neglected.

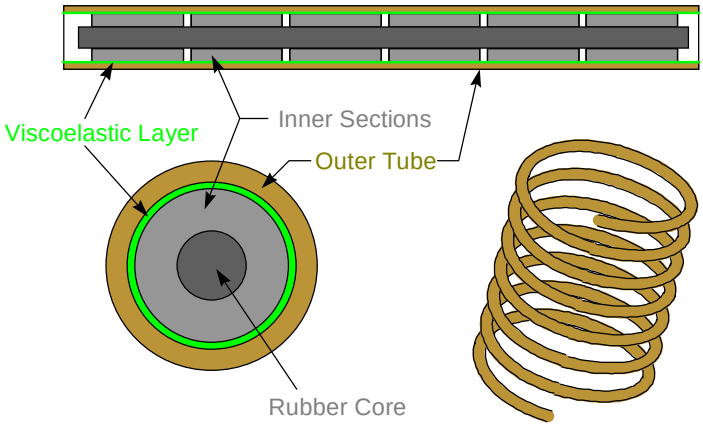

Figure 8: Multi-layer tubular CLD coil spring concept.

Note also that, just like in a classical flat plate CLD design problems[18], there is an optimal length for the constraining layer that maximizes damping, even for a straight CLD torsion bar. The reason for the existence of this optimal length is one of balance between the shear stiffness of the viscoelastic layer and the torsional stiffness (extensional stiffness in a flat plate problem) of the constraining layer. This will be examined in more detail further. The point is that even without geometric coupling, there are performance justifications for using a discontinuous constraining layer instead of a continuous one.

5.2 Analysis

As mentioned in Section 4.2, the state of stress in the cross section of the "wire" of a compression coil spring with a spring index larger than about 5, subject to an axial compression force P is almost identical to that of a straight torsion bar subjected to a twisting moment $T = PD/2$, where D is the mean coil diameter of the spring. With this in mind, we analyze the 3 layer CLD spring by considering the balance of twisting moments

along the length of a single inner constraining section (Fig. 9). The cross section is defined by the inner and outer diameter of the outside tube, d_w and D_w, respectively, the inner and outer diameters of the inside tube sections, d_c and D_c, the shear moduli of the inside and outside tubes, G_c and G_w, and the shear storage modulus and loss factor of the viscoelastic layer, G_v' and η_v. In addition, the following assumptions are made:

- absence of any geometrical coupling between outside and inside tube. This is reasonable as long as the length ℓ of the inner tube sections is much smaller than a full turn of the coil, i.e. $\ell << \pi D$.
- the rubber core is ignored.
- the thickness t_v of the viscoelastic layer is small relative to its mean diameter.
- the axial extent of the gap between inner tube sections is neglected.
- the viscoelastic material is assumed much softer than the inside and outside tube materials, i.e. $G', G_v'' << G_w, G_c$, so that the direct torsional stiffness of the viscoelastic layer can be neglected.

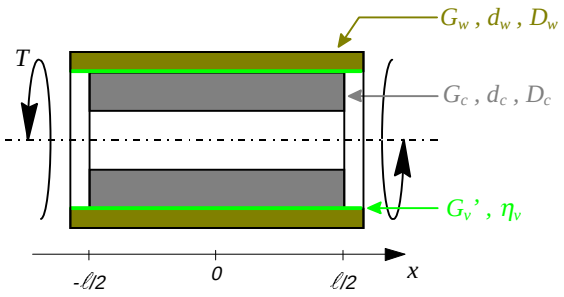

Figure 9: Analysis of straight multi-layer CLD torsion rod.

Writing approximate torsional equilibrium of a "slice" of length *dx* of the 3 layer tube, we have

$$T_w + T_c = T, \tag{13}$$

$$\frac{dT_c}{dx} = G_v'(1+i\eta_v)\frac{\pi d_v^3}{4t_v}(\theta_c - \theta_w), \tag{14}$$

where T_c and T_w are the twisting moments at x in the inner and outer tube cross sections, respectively, θ_c and θ_w are the corresponding twist angles, $t_v = (d_w - D_c)/2$ and $d_v = (d_w + D_c)/2$ are the thickness and mean diameter of the viscoelastic layer, and $i = \sqrt{-1}$.

Using (13), $T_c = G_c J_c \frac{d\theta_c}{dx}$, and $T_w = G_w J_w \frac{d\theta_w}{dx}$, and differentiating (14) we get,

$$\frac{d^2 T_c}{dx^2} - G_v'(1+i\eta_v)\frac{\pi d_v^3}{4t_v}\frac{G_w J_w + G_c J_c}{G_w J_w G_c J_c}T_c = -G_v'(1+i\eta_v)\frac{\pi d_v^3}{4t_v}\frac{T}{G_w J_w}, \tag{15}$$

which is integrated with respect to *x* to get

$$T_c = T\frac{G_c J_c}{G_w J_w + G_c J_c}\left(1 - \frac{\cosh(\lambda x)}{\cosh\left(\lambda\ell/2\right)}\right), \tag{16}$$

and

$$T_w = T\frac{G_w J_w}{G_w J_w + G_c J_c}\left(1 + \frac{G_c J_c}{G_w J_w}\frac{\cosh(\lambda x)}{\cosh\left(\lambda\ell/2\right)}\right), \tag{17}$$

where

$$\lambda = \sqrt{G_v'(1+i\eta_v)\frac{\pi d_v^3}{4t_v}\frac{G_w J_w}{G_w J_w + G_c J_c}}\,. \tag{18}$$

Integrating (17) again we find the inner and outer tube twist angles $\theta_c(x)$ and $\theta_w(x)$, the torsional shear strains and stresses in the inside and outside tubes, the shear strain through the thickness of the viscoelastic layer, and the average torsional stiffness k_t (Nm^2/rd):

$$k_t = \frac{G_w J_w + G_c J_c}{1 + \frac{2}{\lambda\ell}\frac{G_c J_c}{G_w J_w}\tanh\left(\lambda\ell/2\right)}\,. \tag{19}$$

As in Section 4.2.2, the loss factor is then evaluated as $\eta_t = \Im m(k_t)/\Re e(k_t)$.

From Eq. (19), the axial stiffness k_{ax} and loss factor η_{ax} of the coiled spring can be calculated using (5), with the coil geometry defined by the mean coil diameter *D*, and number of turns *n*. Note that $\eta_{ax} = \eta_t$.

5.3 Validation

A 40mm straight length of 3 layer CLD torsion tube was analyzed with NASTRAN (Fig. 10). Both the inside and the outside tube are stainless steel in this example. The mid layer is a hypothetical viscoelastic material with a 50% loss factor. A single layer of quadratic solid elements (20 node bricks) is used to represent each layer of the assembly[19]. The outside tube is supported at one end and loaded with a distributed tangent load at the other; the resultant of the applied loads is an axial torque of 400 Nmm. Figure 10 compares the results from the NASTRAN analysis to those from the closed form analysis presented above. The twist angles of the inside and outside tube are shown as a function of *x* in the top chart (both angles measured with respect to the mid section at *x*=0). The bottom chart shows the "through-the-thickness" shear strain in the viscoelastic layer. Excellent agreement is observed.

As expected, the shear in the viscoelastic layer is maximum at either ends of the inside tube section and corresponds to the local difference in twist angle between the inside and outside tube. The inside tube twists slightly in response to the torque transmitted through the viscoelastic layer. Maximum torsional shear stresses occur at *x*=0 in the inside tube and $x = \pm\ell/2$ in the outside tube.

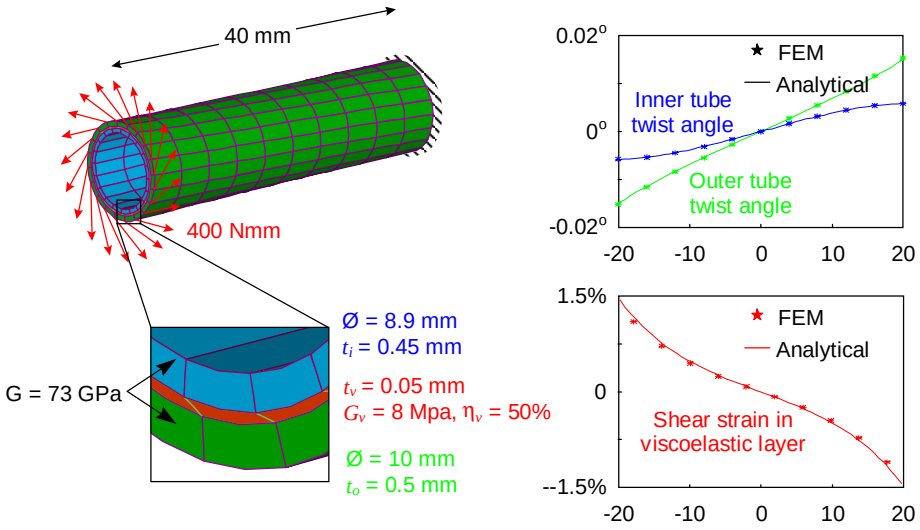

Figure 10: Finite element (NASTRAN) solution for single section of torsion rod compared to closed-form analytical solution.

For validation of the predicted damping ratio, the loss factor of the viscoelastic layer was defined in the NASTRAN model and a large distributed mass was attached to the periphery of the tip of the outside tube in place of the load. This creates a low frequency twisting mode in the torsion tube. A complex eigenvalue solution gives a loss factor for that mode equal to 4.62%. This compares to the 4.68% predicted by equation (19). Also note that a bending mode with a loss factor of 2.2% was found in the NASTRAN solution. This gives an indication of the amount of damping that can be expected in shear deformations of the coiled spring since it involves a combination of torsion and bending in the spring "wire". The shear loss factor of a coiled spring using the cross section of Fig. 10 would then roughly be bounded by the loss factors in torsion and bending of the 3 layer CLD tube, i.e. $2.2\% \le \eta_{sh} \le 4.6\%$.

5.4 Manufacturing and Material Selections

Material selection for this spring design are intimately related to the envisioned manufacturing procedure. Inner tube sections would be cut to length then aligned on a mandrel; the soft viscoelastic layer would then be wrapped and bonded around them. This assembly would then be inserted into a slightly oversized outer tube (after being spread with an adhesive) which would be swaged around it. This creates a length of straight multi-layer torsion tube that must be coiled on a mandrel. Stresses created by the coiling must then be relieved through a low temperature heat treatment.

Some critical aspects of this procedure and their implications on the design and material selections are described below.

5.4.1 Deformation of inner sections during coiling

During coiling, there will be a tendency for the edges of the inner tube sections to dig into the soft viscoelastic layer. To reduce the chances of this happening, a soft (low yield point) material should be used for these inner tube sections. We have tentatively

selected a soft aluminum alloy. Another concern is potential wrinkling of the inner tubes, which might require a stiffer alloy. A compromise will have to be found.

5.4.2 Tube support during coiling

Coiling a tube to a relatively tight mean coil diameter is a tricky operation: well designed support tools must be used to prevent excessive flattening which would "lock" the relative twist between inside and outside tubes and eliminate damping.

We are considering an option where the inside sections would be aligned on a solid rubber core that would remain inside the tube in the final coil (as shown in Fig. 8). The rubber core would provide internal support to the cross section during coiling and help avoid excessive flattening. The rubber would have to be soft enough to not create excessive coupling between successive inner tube sections.

5.4.3 Viscoelastic material

To maximize damping, the visco-elastic layer must be as thin as possible. However, extremely thin layers are difficult to handle and would require extreme tolerances on the diameters of the tubes and the swaging operation. A thickness of the order of 10 mils (0.25mm) is considered a minimum.

Design studies show that with thicknesses greater than 10 mils, typical self adhesive acrylic damping layers like 3M's Scotchdamp[20] are too soft (*G'* of the order of 0.3 MPa at 10 Hz) to provide sufficient damping. A relatively stiff viscoelastic material is required (damping is controlled by the factor $G'_v \eta_v d_v^3 / t_v$, see Section 5.2). DYAD 606[12] manufactured by Soundcoat was selected. It is available in 20 and 50 mil thicknesses, has very high loss factor and relatively large shear modulus at low frequency (105% at 10 Hz), and is pliable enough for wrapping around the inner tube sections. This material is not self adhesive. A flexible epoxy glue must be used bond it to the metal surfaces.

5.4.4 Coiling strains and selection of outer tube material

Large strains are induced at the outside fibers of the outside tube during coiling and must be relieved by heat treatment. The material used for the outside tube must therefore be pliable enough to avoid cracking. Since the outside tube is also the load bearing component for the static load, a compromise must be found between high yield and formability. It would be tempting to use an age-hardenable alloy (beryllium copper for example) that could be coiled in the annealed condition then hardened by heat treatment. Unfortunately, the temperatures required for age hardening (550°F minimum) are incompatible with the presence of the viscoelastic layer. The selection of a material is then driven by the stress relief temperature required and its compatibility with the maximum temperature sustainable by the visco-elastic layer. Soundcoat's DYAD 606 can sustain temperatures up to 350°F for several minutes. Of all metals appropriate for cold wound coil springs, phosphor bronze has the lowest stress relief temperature at about 325°F[10]. It is available in various mill tempers obtained by cold work. For good spring properties (high yield) the hardest possible temper should be used. However, hard tempers have low ultimate strains and are more likely to crack during coiling. The maximum coiling strain in the outside tube ε_w^{coil} is a function of the spring index *c* and can be estimated to fall within the interval

$$\frac{1}{c} \le \varepsilon_w^{coil} \le \frac{2}{c}. \qquad (20)$$

For spring indices around 5, this gives coiling strains between 20 and 40%. Phosphor bronze tubes in annealed, ¼ hard, ½ hard, and ¾ hard tempers have ultimate strains of about 55, 50, 35, and 21 %, respectively, and yield strengths of about 51.1, 51.4, 53.0, and 64.1 ksi, respectively[21]. Test coils (using a solid rubber core for internal support) will be produced using these 4 tempers in an effort to determine the hardest temper compatible with the coiling operation.

5.5 Design Optimization

Looking at the relations in Section 5.2, it is apparent that optimal proportions must exist for the diameters and thicknesses of the 3 layers that maximize net damping. A simple trend study was performed to get an idea of the effects of the various design parameters. The results of that study are summarized in Fig. 11.

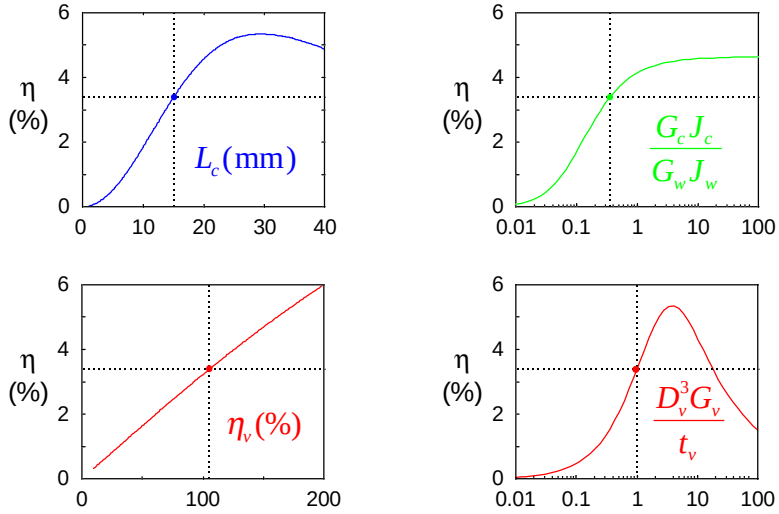

Figure 11: Effect of various cross section parameters on net torsional damping.

The four curves in the figure show the individual effects of 4 parameters on the torsional damping: the length of the inner tube sections L_c, the torsional stiffness balance between the inner and outer tubes $G_c J_c / G_w J_w$, the loss factor of the viscoelastic layer η_v, and the stiffness measure of the viscoelastic layer $D_v^3 G_v / t_v$. These parameters were varied one at a time around a nominal configuration of aluminum, DYAD 606, and phosphor bronze, with D_w = 6 mm, t_w = 0.5 mm, t_v = 0.25 mm, and solid inner sections of aluminum rod, with L_c = 15 mm.
The following observations can be made:

- damping is very sensitive to L_c. Physically this is explained as follows: when L_c is large, load transfer to the inner sections accumulates along their length and forces them to twist, reducing the twist angle differential and the damping. If the sections are short, the twist angle differential at their ends is small and damping is again small. An optimal

length (about 30 mm in this case) exists that maximizes damping. Note that this optimal length also depends on the values of the other 3 parameters.

- the torsional stiffness of the core must be large enough to minimize twist in the inner sections. The figure shows that for $G_c J_c / G_w J_w$ greater than about 1, the effect of this parameter is small.
- as expected, an increase in the loss factor of the viscoelastic layer leads to an almost proportional increase in net spring loss factor.
- the effect of the viscoelastic layer "stiffness" $D_v^3 G_v / t_v$ also shows the existence of an optimal value. This is again explained by a balance condition between a stiff layer that induces too much twist in the inner section, reducing shear strains and damping, and a soft layer with which twist of the inner sections is minimized but the strain energy in the viscoelastic layer is reduced because of its low modulus and/or large thickness.

Since many different variables have strong effects on the spring final performance and the trend study shows the existence of optimal values, we used numerical optimization techniques to lead us to favorable proportions for the cross section and coil geometries. The objective is to maximize characteristic deflection $\delta_{\max}$ of the spring while providing at least 3% damping and satisfying a number of additional conditions. The static load capacity was evaluated in such a way that no damage is done to the spring by compressing it solid. The optimization problem was formulated as follows:

ADJUST

cross section geometry: d_c, t_c, t_w

constraining section length: L_c

Coil Geometry: active length L, pitch p, mean coil diameter D

WITH

$0 \text{ mm} < d_c < 5 \text{ mm}$, $0.3 \text{ mm} < t_c < 3 \text{ mm}$, $0.5 \text{ mm} < t_w < 3 \text{ mm}$

$5 \text{ mm} < L_c < 50 \text{ mm}$

$10 \text{ mm} < L < 80 \text{ mm}$, $1 \text{ mm} < p < 20 \text{ mm}$, $10 \text{ mm} < D < 80 \text{ mm}$

TO MAXIMIZE

characteristic deflection $\delta_{\max}(35 \text{ Hz})$

SUCH THAT

net loss factor $\eta\,(35 \text{ Hz}) > 3\%$

Number of section per turn $\pi D / L_c > 6$

Spring index $c = D / D_w > 5$

pitch angle $\alpha < 12°$

active turns $n = L/p > 2$

viscoelastic layer diameter to thickness ratio $D_v / t_v > 10$

first resonant frequency $f_1 > 400$ Hz

active length to coil diameter ratio (buckling) $L / D < 2.5$

Static load capacity 100 lbs $< P_{\max} < 300$ lbs

max. active length $L < 50$ mm

where the cross section is defined by the ID of the inner tube sections d_c, and the wall thicknesses of the inner and outer tubes t_c and t_w, respectively. The viscoelastic layer thickness is not taken as a design variable because DYAD 606 is available only in discrete thicknesses (20, 50, and 100 mils). To maximize damping, we selected a 20 mil (0.508 mm) layer.

The analysis was coded in MATLAB and the optimization problem was solved using MATLAB's multivariable constrained minimization routine.

5.6 Final Design

Final cross sectional dimensions and coil geometry resulting from optimization are shown in Fig. 12. To the 2.3 active turns called for by the optimizer, we have to add end coils to provide interface with the stack elements. Because of the tubular cross-section and the small axial clearance between coils, achieving flat end coils normal to the spring axis is not possible. Instead, seats are used to provide support at each end of the spring. The design of those seats and the material used are not yet completely determined. Prototyping is expected to lead to a final design. Note also that, if these springs show acoustic transmission problems, the seats could be made of VITON and play the role of an acoustic pad. Alternatively, thin VITON "washers" could be inserted between the seats and the stack elements.

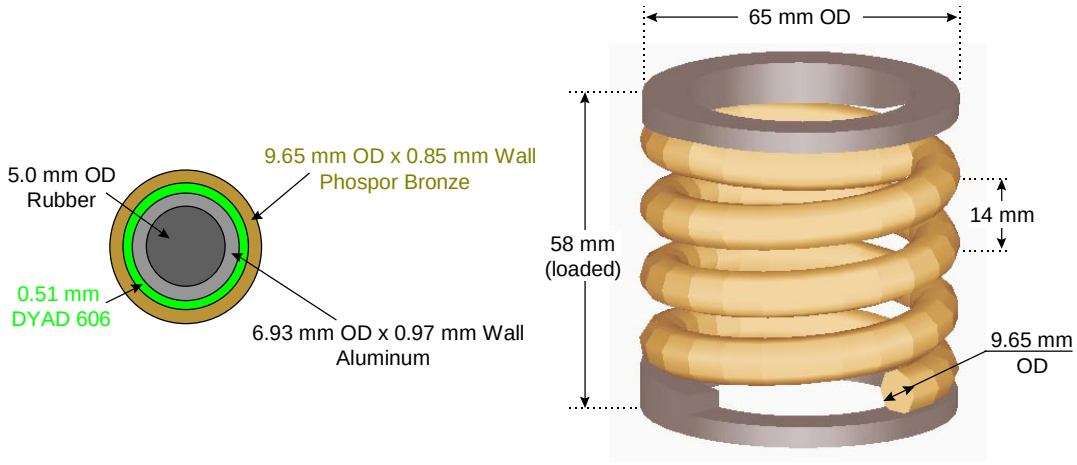

Figure 12: Final design of CLD coil spring; the seats at the spring-stack element interface could be made of Viton for acoustic padding.

5.7 Performance

Analysis of this design provides the frequency dependent axial stiffness and loss factor shown in Fig. 13. Shear stiffness and loss factor are much harder to predict because they involve complex combinations of bending and torsion of the cross-section. Short of adequate analysis, a fixed ratio k_{sh}/k_{ax} of 40% (typical for heavy-duty compression coil springs) was assumed at all frequencies. The shear loss factor was assumed to be 75% of the axial loss factor (see section 5.3).

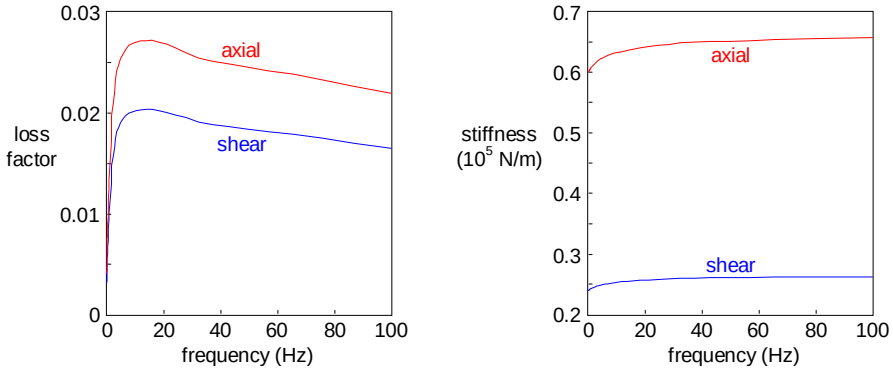

Figure 13: Predicted axial and assumed shear properties (stiffness and loss factor) of the coil CLD spring.

Simulation of a BSC stack using those springs provides the predicted isolation levels of Fig. 14. The requirements from the draft DRD document[2] are shown in red. Note that the vertical isolation requirement is satisfied with a comfortable margin while horizontal isolation is just sufficient. Remember however that T_{xx} predictions are dependent on the assumed shear stiffness of the springs.

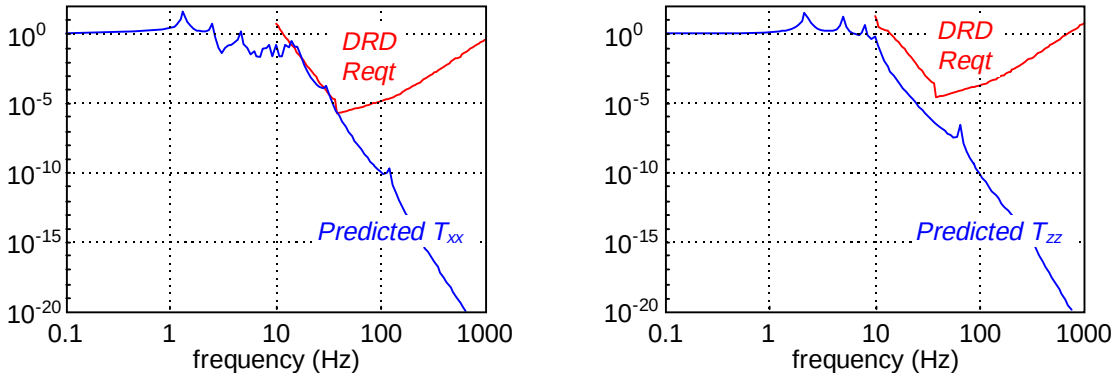

Figure 14: Predicted horizontal (left, blue) and vertical (right, blue) isolation of BSC/SEI with CLD coil springs. Draft DRD requirements are shown in red.

6. Semi-Circular Leaf Spring with Constrained Layer Damping

The complex manufacturing procedure required for the coil CLD spring and the lack of experience with this type of structure prompted us to develop a different concept, using more conventional techniques and materials.

6.1 Concept

The spring consists of a semi circular blade of radius *R*, sitting on end and supporting the static load *P* along its main diameter (see Fig. 15). The lower end of the blade is clamped in place, restricting all displacements and rotations at that end. The upper end receives the vertical static load (weight of the rest of the stack). The blade is a

sandwich of metal leaves and a thin viscoelastic layer acting as a constrained layer damping treatment.

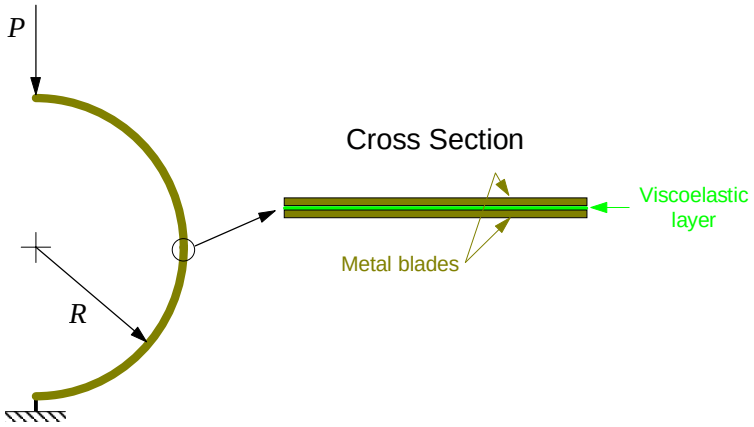

Figure 15: CLD leaf spring concept.

Because of the asymmetry of the spring, the tip displacement under load is not purely vertical (Fig. 16). This would lead to large vertical-horizontal coupling, undesirable in the isolation stack design.

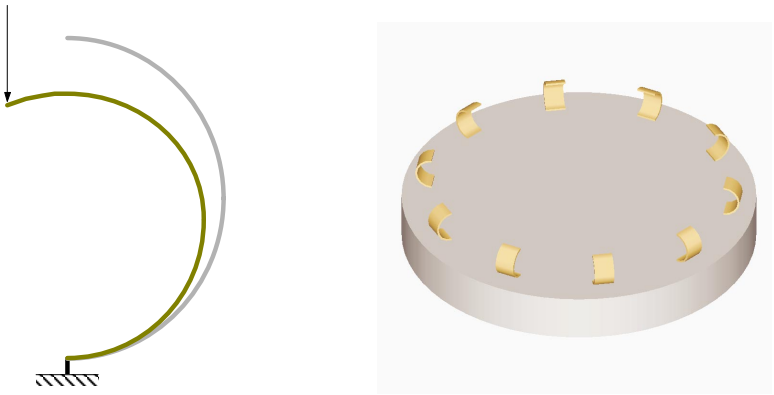

Figure 16: asymmetric deflection of unrestrained leaf spring and spring arrangement to prevent it .

However, this coupling can be globally “averaged out” by arranging and orienting the springs of each stage symmetrically around the axis of the stack leg as shown in Fig. 16.

As mentioned before, any viscoelastic material must be completely enclosed within the metal spring. Obviously, the conceptual design of Fig. 15 does not meet that requirement. Closing the cross section by welding together the edges of the two blades would lock shear deformations in the viscoelastic layer, eliminating damping. One option to reconcile these requirements is to use multiple layers and weld together the edges of the outermost layers. For ease of fabrication, the number of layers should be kept to a minimum. With 3 metal layers (Fig. 17.a), classical bending theory predicts zero shear in the damping layers (for a symmetric cross-section). In contrast, a 4-layer sandwich (Fig. 17.b) creates shear deformations in all 3 damping layers in response to bending.

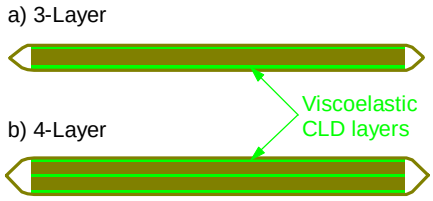

Figure 17: Cross sections of sealed CLD leaf springs with 4 and 4 layers.

To further simplify the cross-section and because the neutral axis of a curved beam is offset toward the center of curvature, the cross section was made asymmetric by bending the sides of the inner shell only (Fig. 18). With this design, 3 of the 4 metal blades can simply be bent into shape while the inner shell is stamped. The half circle is extended at each end with a flat section for clamping and load interface. The spring geometry is designed slightly "open" so that the tip is as close as possible to horizontal under full static load. The upper end is fitted with a small VITON pad that serves two distinct purposes:

1. it provides a somewhat uniform transfer of the static load into the spring, allows for minor misalignment of the tip with respect to the stack element under load and creates a "hinge" that allows twist and rocking dynamic deflections of the spring tip.
2. it serves as an acoustic pad, blocking high frequency perturbations that may not be adequately damped by the CLD layers.

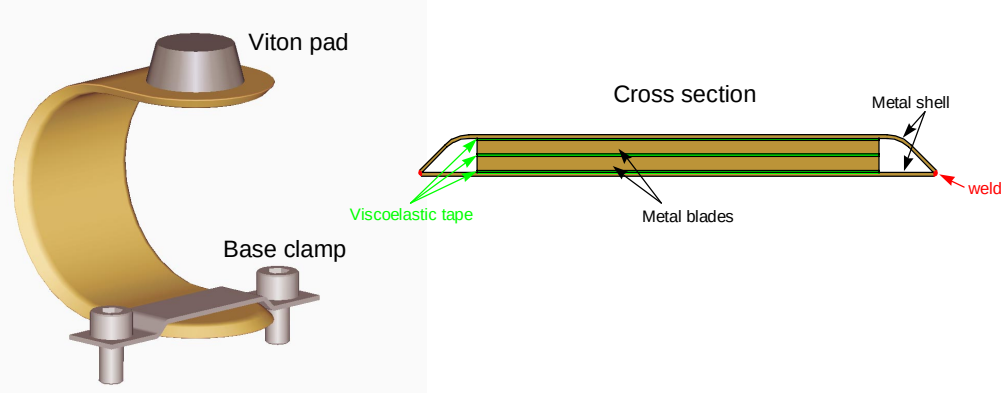

Figure 18: Conceptual design of the semi-circular CLD leaf spring.

6.2 Manufacturing Procedure

As stated at the beginning of this section, manufacturing of this leaf spring is expected to be substantially simpler than that of the coil CLD spring of section 5. The basic operations would consist of:

1. cutting all metal sheet and viscoelastic tape pieces to shape.
2. forming all metal parts: stretch bending for all flat blades and stamping for the inner shell are envisioned[22]. These operations are followed by thorough cleaning of the metal surfaces.
3. assemble the spring layer by layer, using self adhesive viscoelastic tape.

4. weld the edges of the inner and outer shells together. Heat sinks will be required to keep the viscoelastic layers at low temperature during this operation. Laser or E-beam welding are being considered.
5. Install clamp and Viton pad, clean.

6.3 Material Selections

6.3.1 Outer shell and internal blades

A pliable material is desirable from a manufacturing point of view (ease of bending and stamping operations). However, as with the coil spring of section 5, resistance to high static stresses requires a high yield material. Since all forming operations can be completed before addition of the CLD layers, an age-hardening material like Beryllium Copper is an appealing option: it can be shaped in its annealed form, then age-hardened by heat treatment at about 600ºF for a few hours. Its yield strength after hardening is around 1250 MPa[23].

6.3.2 Viscoelastic CLD layers

A self adhesive CLD layer was selected to simplify the assembly procedure. 3M Scotchdamp damping layer is available in thicknesses of 2 mils, 5 mils, and up, is self adhesive and is used extensively as a thin shell CLD layer in the aerospace industry. Because the 2 mil tape is extremely fragile and delicate to apply, we tentatively selected a 5 mil (0.127 mm) thickness.

6.4 Final Design

Although no formal optimization was conducted for this design, a few design iterations with FEM analysis led to the geometry and dimensions of Fig. 19.

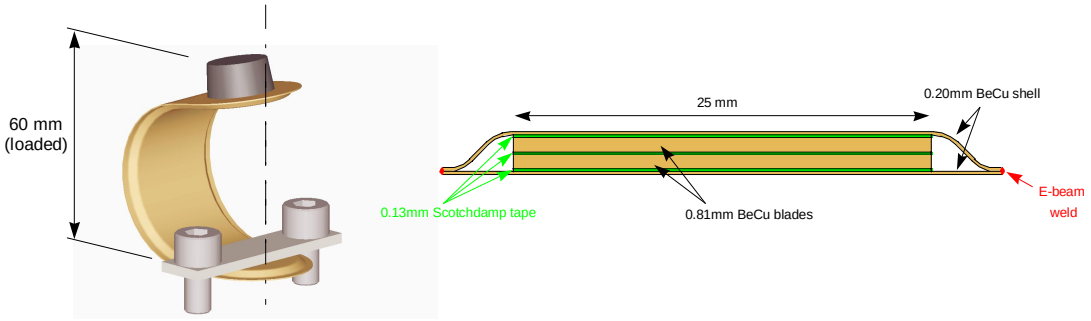

Figure 19: Dimensions of semi-circular CLD leaf spring.

Exact designs of the clamping mechanism and Viton pad have not been finalized. Prototyping and testing is expected to provide vital information for these aspects of the design.

6.5 Static Analysis

Average stresses can be roughly evaluated with classical bending theory, neglecting curvature. The applied load and the support reactions create a bending moment distribution along the spring that can be evaluated numerically (MATLAB). Assuming again that the viscoelastic layers do not contribute any DC stiffness (because they creep), we can then evaluate the maximum Von Mises stress in the cross section as a function of

the angular coordinate α. These results (combining bending and direct compression stresses) are shown in Fig. 20 for a static load of 556 N (125 lbs). The spring was purposely designed to this static capacity so as to constitute a direct one-to-one replacement for the Viton springs. The figure also shows the yield strength of age-hardened beryllium copper. A safety factor of about 1.4 is observed.

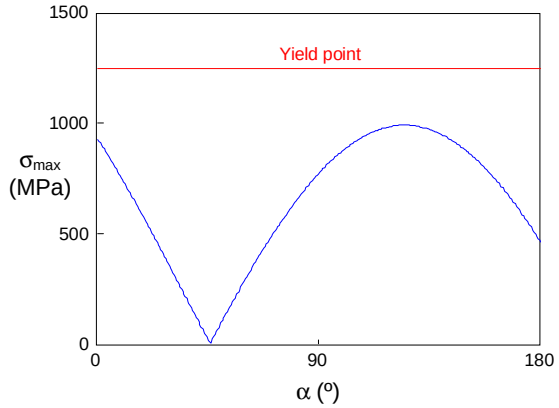

Figure 20: Approximate static Von Mises stresses in outer shell.

Finite element results confirm the results from this simple analysis but reveals stress concentrations in the area of the bend in the inner shell. These concentrations can be greatly reduced by presetting the springs before use (loading them to more than full capacity, which produces localized yielding in the stress concentration areas; this causes residual stresses to appear in those areas; these residual stresses then oppose the working stresses, preventing further plastic deformations).

6.6 Dynamic Analysis

Stiffnesses and loss factors are evaluated as a function of frequency in the axial and shear directions. Note that since the spring is asymmetric, two distinct shear directions must be considered: a “rolling” shear deformation and a “twisting” shear direction (Fig. 21).

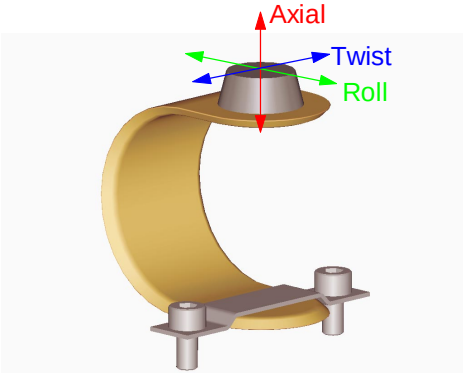

Figure 21: Axial and shear deformations of the leaf spring.

A very simplified finite element model (Fig. 22) was created in NASTRAN using a single layer of solid quadratic elements (20 node bricks) per layer of beryllium copper or viscoelastic material. Only the ½ circular part of the spring was modeled. The tip extensions were represented as rigid links (multi-point constraints) connecting the ends of the outer shell to the load application points. The effect of the Viton pad was not taken into account.

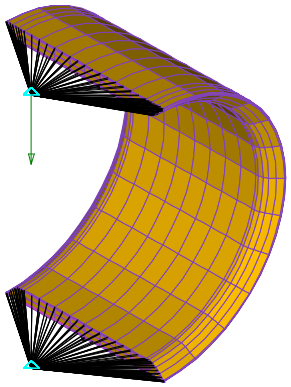

Figure 22: Finite element model of the leaf spring

Frequency dependent material properties were defined for the viscoelastic layers. Stiffnesses and loss factors were evaluated at 5 discrete frequencies (1, 10, 30, 50, and 100 Hz). Unit loads were applied at the tip in the direction of interest (locking the other 2 degrees of freedom) and the tip displacement (a complex number) was evaluated or each frequency. Simple calculations then provide the stiffness and the loss factor. These results are plotted in Fig. 23.

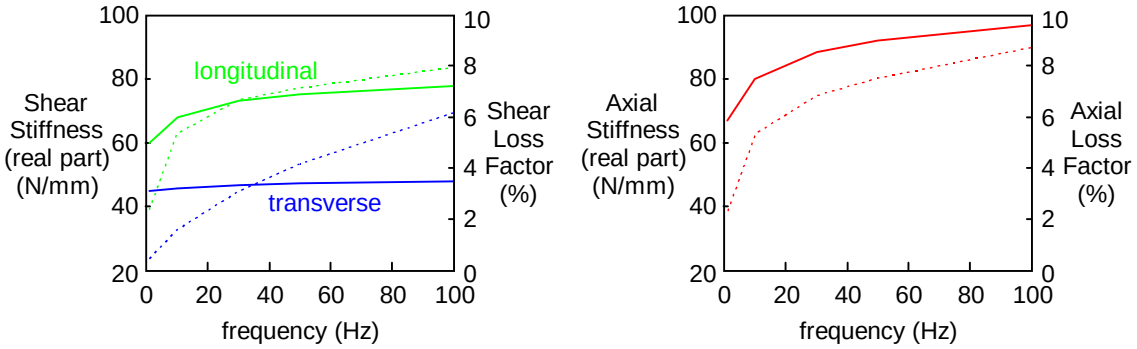

Figure 23: Predicted axial and shear stiffnesses (solid curves) and loss factors (dashed curves) of CLD leaf spring.

6.7 Performance

The frequency dependent stiffnesses and loss factors shown above are introduced into the 3D MATLAB simulations of the BSC/SEI. Note that the shear behavior of the springs was assumed isotropic in the simulations. Isotropic shear stiffness and loss factor were obtained by averaging the complex stiffnesses corresponding to the roll and twist deformations. Predictions of the vertical and horizontal transmissibilities are shown in Fig. 24.

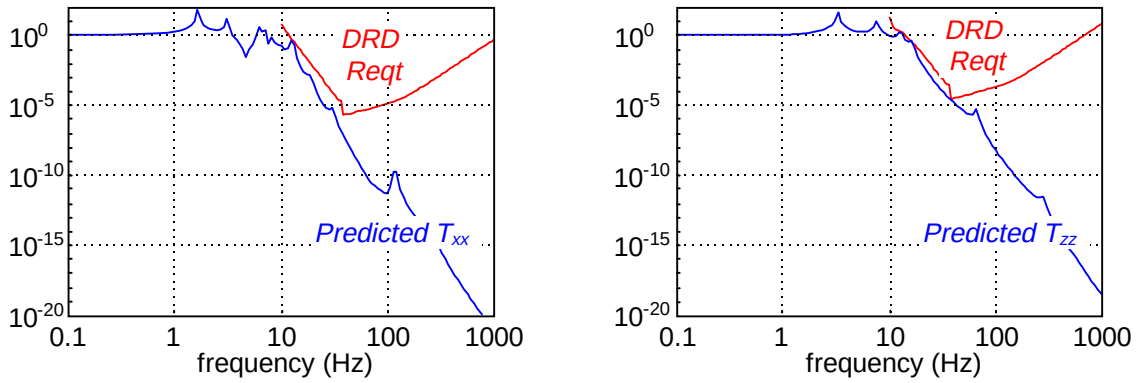

Figure 24:Predicted axial and shear stiffnesses (solid curves) and loss.

Again, these results show that these springs have the potential of providing sufficient vertical and horizontal isolation to satisfy the requirements.

7. Conclusions and Future Work

We have arrived at two different metal spring designs that - on paper - achieve the main goals: provide sufficient isolation with a metal spring with internal damping treatments completely isolated from the vacuum environment. Approximate static and dynamic analyses have provided estimates of these spring's performance. Their static load capacity and size has been kept close to those of the Viton springs so that substitution of one type of spring for another in the final stages of preliminary design of the SEI will be possible. The design of those springs is seriously complicated by the requirement of complete enclosure of viscoelastic materials within a vacuum tight metal envelope calling for unusual manufacturing techniques.

A number of critical issues remain to be examined. They concern manufacturability and cost on one side and acoustic transmission, vacuum compatibility, creep and creak under load, and experimental verification of static, dynamic, and buckling properties on the other. To answer these questions, we propose to conduct prototyping and experimental testing programs. The testing will be scheduled in a step by step fashion, starting with the simplest tests of the most critical issues and leading to more refined and complex tests duplicating the actual operating conditions (in vacuum, extremely small amplitudes,…). Failure at any of these stages would exclude the particular spring design.

In addition, it now appears necessary to examine stack behavior in more detail: the effects of imperfections (misalignments,…) and variability in spring properties on vertical-horizontal coupling in the stack for example. Also, a more realistic modeling of the arch springs, including the non-isotropic shear behavior and axial-shear coupling must be integrated into the stack simulations.

8. References

1. E. Ponslet, *Isolation Stacks Preliminary Design Methodology*, HYTEC Inc., Los Alamos, NM, document HYTEC-TN-LIGO-02, February 21, 1996.

2. F. Raab and N. Solomonson, *Seismic Isolation Design Requirements Document* (draft and early corrections), LIGO draft document LIGO-T960065-02-D, California Institute of Technology and Massachusetts Institute of Technology, April 15, 1996.
3. E. Ponslet, *BSC Stack Design Trend Study*, HYTEC Inc., Los Alamos, NM, document HYTEC-TN-LIGO-03, March 1st, 1996.
4. Associated Spring/Raymond, Barnes Group Inc., 1705 Indian Wood Circle, Suite 210, Maumee, OH 43537-4046, (800) 872-7732.
5. W. Young *et al*, *LIGO Vacuum Compatibility, Cleaning Methods and Procedures* (draft), LIGO draft document LIGO-E960022-00-D, California Institute of Technology and Massachusetts Institute of Technology, February 26, 1996.
6. P. R. Saulson, *Fundamentals of Interferometric Gravitational Wave Detectors*, World Scientific, River Edge, NJ, 1994.
7. C. M. Harris, *Shock and Vibration Handbook*, 3rd edition, McGraw-Hill, 1988.
8. W. Dejonghe, L. Delaey, R. De Batist, and J. Van Humbeeck, "Temperature- and amplitude-dependence of internal friction in Cu-Zn-Al alloys," *Metal Science,* pp. 523-530, November 1977.
9. J. Beyer and M. Chandrasekaran, "On the Stability of Shape Memory Alloy Materials and their Properties in Static and Dynamic Applications," in *Smart Structures for Aircraft and Spacecraft*, AGARD-CP-531, Proceedings of the 75th Meeting of the AGARD Structures and Materials Panel, Lindau, Germany, pp. 13-1 to 13-7, October 5-7, 1992.
10. A. M. Wahl, *Mechanical Springs*, 2nd edition, McGraw-Hill, 1963.
11. *S.A.E. Manual on Design and Application of Helical and Spiral Springs,* SAE HS-795, SAE, Warrendale, PA, 1996.
12. Soundcoat® Product Data Sheet, Bulletin 701, *DYAD for use in Thick Plate Vibration Damping*, and Bulletin 810, *Constrained Layer Damping Materials for Control of Noise and Vibration*, Soundcoat®, 1 Burt Dr., Deer Park, NY 11729.
13. Sorbothane® Damping Characteristics, Web page (http://www.sorbothane.com), Sorbothane Inc., 2144 State Route 59, Kent, OH 44240.
14. Technical Data Sheets, EAR Specialty Composites, Cabot Safety Corp., 7911 Zionsville Road, Indianapolis, IN 46268.
15. VEM Database v1.10, WL/FIBG Bldg 24C, 2145 5th St., Ste 2, Wright-Patterson AFB, OH 45433-7006.
16. Viton reference ????
17. D. Vautour, *Vibration Damping Test Results on LNP Thermoplastics*, LNP Engineering Plastics, Campbell Blvd & Creamery Way, Exton, PA 19341.
18. R. Plunkett and C. T. Lee, "Length Optimization for Constrained Layer Damping," *Journal of the Acoustical Society of America*, Vol. 48, No. 1 (part 2), pp. 150-160, 1970.
19. C. D. Johnson and D. A. Kienholz, "Finite Element Prediction of Damping in Structures with Constrained Layer Viscoelastic Layers," *AIAA Journal*, September 1982, pp. 1284-1290.
20. Scotchdamp™ Product Information, 3M Vibration Control, 3M Center, Building 230-1f-02, St Paul, MN 55144-1000.

21. Small Tube Products Co., Inc., Altoona, PA, test results on phosphor bronze tubes (private communication), June 1996.
22. *Metals Handbook,* 8th edition, Vol. 4: Forming, T. Lyman, Ed., ASM, Metals Park, OH 44073.
23. *Beryllium Copper Heat Treatment,* NGK Berylco, NGK Metals Corp., P.O. Box 13367, Reading, PA, 19612.

Note 1, Linda Turner, 09/03/99 11:28:48 AM
LIGO-T960212-A-D